One Policy but Many Worlds: A Scalable Unified Policy for Versatile Humanoid Locomotion

Yahao Fan 1,* Tianxiang Gui 1,* Kaiyang Ji 1,* Shutong Ding 1,2 Chixuan Zhang Jiayuan Gu 1,2 Jingyi Yu 1,2 Jingya Wang 1,2,† Ye Shi 1,2,†

 $1ShanghaiTech University <math display="inline">^2MoE Key Laboratory of Intelligent Perception and Human Machine Collaboration

{fanyh12024, v-guitx, jiky2024}@shanghaitech.edu.cn {dingsht, zhangchx12024, gujy1}@shanghaitech.edu.cn {yujingyi, wangjingya, shiye}@shanghaitech.edu.cn

Abstract

Humanoid locomotion faces a critical scalability challenge: traditional reinforcement learning (RL) methods require task-specific rewards and struggle to leverage growing datasets, even as more training terrains are introduced. We propose Dream-Policy, a unified framework that enables a single policy to master diverse terrains and generalize zero-shot to unseen scenarios by systematically integrating offline data and diffusion-driven motion synthesis. At its core, DreamPolicy introduces Humanoid Motion Imagery (HMI) - future state predictions synthesized through an autoregressive terrain-aware diffusion planner curated by aggregating rollouts from specialized policies across various distinct terrains. Unlike human motion datasets requiring laborious retargeting, our data directly captures humanoid kinematics, enabling the diffusion planner to synthesize "dreamed" trajectories that encode terrain-specific physical constraints. These trajectories act as dynamic objectives for our HMI-conditioned policy, bypassing manual reward engineering and enabling cross-terrain generalization. Crucially, DreamPolicy addresses the scalability limitations of prior methods: while traditional RL fails to exploit growing datasets, our framework scales seamlessly with more offline data. As the dataset expands, the diffusion prior learns richer locomotion skills, which the policy leverages to master new terrains without retraining. Experiments demonstrate that DreamPolicy achieves an average of 90% success rates in training environments and an average of 20% higher success on unseen terrains than the prevalent method. It also generalizes to perturbed and composite scenarios where prior approaches collapse. By unifying offline data, diffusion-based trajectory synthesis, and policy optimization, DreamPolicy overcomes the "one task, one policy" bottleneck, establishing a paradigm for scalable, data-driven humanoid control. Anonymous project page of our work is provided in https://dreampolicy.github.io/.

1 Introduction

The rapid advancement of embodied intelligence has positioned legged robots as pivotal agents for bridging virtual intelligence with physical-world interactions, particularly in scenarios requiring dynamic balance [1, 2], dexterous manipulation, and adaptive locomotion. Recent advances in legged locomotion have enabled quadrupedal robots to perform dynamic tasks such as parkour [3, 4, 5, 6]

^{*}Equal contribution. †Corresponding author.

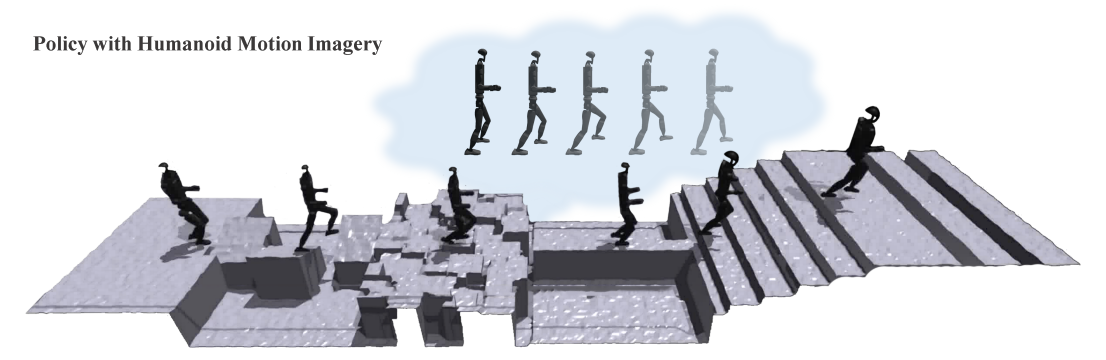


Figure 1: The policy learns to imagine terrain-aware humanoid motions (HMI), enabling zero-shot generalization to challenging terrains without task-specific rewards.

and whole body loco-manipulation [7, 8]. Humanoid robots, with their anthropomorphic design, hold immense potential for operating in human-centric environments, from locomotion [9, 10, 11] to manipulation [12, 13], even whole-body loco-manipulation tasks [14, 15, 16, 17, 18].

Notably, the majority of these works struggle with generalization to various complex scenes. To better exploit the morphological advantages of humanoid robots and achieve more human-like and natural motion, recent approaches incorporate pre-trained models [19, 20] or human motion priors [16, 21, 22, 23] to guide policy learning. These priors reduce the exploration burden in reinforcement learning and encourage the discovery of more feasible action spaces. However, how to generalize these capabilities to diverse challenge scenarios (e.g., slopes, gaps, uneven terrain) and external disturbances [9, 11, 24, 25, 26] remains an open challenge. Specifically, most learning-based approaches tend to overfit to specific training conditions (e.g., stair climbing, inclined surfaces [27, 28]), conduct task-related rewards, and are hindered by inefficient exploration due to algorithm-environment coupling. Moreover, policy distillation [4] aggregates specialized skills into a unified policy, but it inherits the brittleness of its constituent experts. Moreover, online distillation requires continuous interaction with costly simulators and struggles to generalize beyond curated training distributions. Hence, designing a unified policy capable of handling humanoid locomotion tasks across a variety of terrains is of exceptional importance.

To address these challenges, we propose **DreamPolicy**, a novel framework that augments conventional reinforcement learning through synergistic integration of a terrain-aware autoregressive diffusion planner. Our approach introduces Humanoid Motion Imagery (HMI) - future state predictions synthesized by a diffusion model trained on aggregated expert demonstrations. HMI serves as an implicit, terrain-adaptive reward signal that helps DreamPolicy generalize to novel terrains. The framework operates in three stages: First, we train specialized RL policies across six distinct terrains, generating a diverse Humanoid kinematic dataset through large-scale simulation. Subsequently, we train an autoregressive Diffusion Planner on this dataset to model cross-scenario state-action distributions, enabling probabilistic synthesis of physically plausible trajectories. Finally, we optimize a physics-constrained RL policy conditioned on HMI, using the diffusion planner's predictions as dynamic objectives that balance trajectory tracking accuracy with physical realism. This decoupled architecture allows continuous improvement through dataset expansion while eliminating manual reward engineering.

The contributions of our work could be summarized as follows:

- **DreamPolicy: Unified Policy for Cross-Terrain Locomotion.** A framework that enables a single policy to achieve robust humanoid locomotion across various scenarios without complex reward engineering or policy distillation. DreamPolicy achieves this by combining primitive skills collection, humanoid motion imagery via a terrain-aware autoregressive diffusion planner, and HMI-conditioned RL policy, thereby eliminating the need for intricate reward design in cross-terrain generalization.
- Terrain-aware Humanoid Locomotion Primitive Skills Collection. We collected terrainspecific locomotion primitive skills via trained specialized policies in six distinct single-terrain environments and aggregated their rollouts. Unlike human motion datasets requiring laborious retargeting, our dataset directly captures humanoid kinematics and dynamics across diverse terrains, enabling efficient learning of terrain-adaptive motion priors.

- Scalable Diffusion-driven Humanoid Motion Imagery for Policy Generalization. Traditional humanoid locomotion methods struggle to scale with abundant data due to their reliance on handcrafted rewards and fragmented training. DreamPolicy addresses this limitation by leveraging a diffusion-based Humanoid Motion Imagery (HMI) trained on offline humanoid datasets. HMI generates terrain-adaptive trajectories and scales effectively with larger datasets, allowing RL policies to generalize without complex reward engineering. By decoupling motion synthesis from policy optimization, DreamPolicy fully exploits large-scale offline data to enhance policy robustness.
- Robust Generalization & Empirical Validation. Despite training on only six single-terrain types, DreamPolicy achieves a 90% average success rate in single terrains and successfully generalizes to unseen and combined terrains, outperforming the prevalent method by an average of 20%. Extensive evaluations confirm its strong zero-shot adaptation using offline data, effectively overcoming the scalability limitations of traditional approaches.

2 Related Work

2.1 Humanoid Locomotion

Legged locomotion control has been studied extensively, especially humanoid locomotion. Recent advances in humanoid robotics [9, 13] have demonstrated the potential of humanoid robots. Existing works like Extreme Parkour [3], Distillation-PPO [29] and [9] employs a hierarchical framework for humanoid skill learning, works such as DWL [27] and Humanoid Perception Controller [30] extract the latent state of sensors and reconstruct the true state, these works aiming to alleviate the Sim2Real gap. However, the majority of these works depend on labor reward engineering, to this end, works like Teacher Motion Prior [31], H2O [22], and OmniH2O [32] leverage human motion datasets and retarget to humanoid datasets, which leverages the morphology advantage of humanoid. Unlike these works that depend on retargeted human datasets (e.g., AMASS [33]), our collected skills preserve native humanoid kinematics. This approach eliminates the need for manual reward design while ensuring scalability: generalization of the policy becomes stronger as the data scales up, addressing the "one task, one policy" bottleneck inherent to traditional RL.

2.2 Unified Policy for Robot Control

Integrating cross-scenario and cross-embodiment skills into unified policy frameworks has emerged as a prominent approach for enhancing control system robustness and responsiveness. Recent works [34, 35, 36] address encoded common environment factors via unified goal or action representations which bridge cross-scenario tasks. Some studies [37, 38, 39, 40, 41, 42], like SMP [38] and URMA [40], focus on robotics morphological differences such as parameterized link/joint configuration to mitigate structural disparities across platforms. In the field of learning foundation models for robotics, researches like Octo [43], GR00T N1 [44], RT-1 [45], RT-2 [46] demonstrate that scaling training data substantially improves cross-setting generalization. The most directly comparable work, Robot Parkour Learning [4], employs online distillation to unify several terrain-specific policies. While existing approaches predominantly address either cross-embodiment adaptation or robotic arm manipulation, our framework introduces an autoregressive diffusion model that predicts future state-action trajectories on unseen-scenario locomotion task. This architectural innovation reduces policy generalization burden while enabling humanoid robots to achieve enhanced environmental adaptability and operational versatility in complex scenarios.

2.3 Diffusion Models for Robot Learning

Recent years have seen diffusion models transition from image [47, 48, 49] and video [50, 51] synthesis into the domain of robot learning [52, 53, 54]. Diffusion models have been widely adopted across imitation learning [52, 53, 55], offline RL [56, 57, 58] and online RL [59, 60, 61]. Rather than generating actions stepwise, diffusion planners produce entire trajectories by denoising noise [62, 63, 64], which naturally supports long-horizon planning conditioned on task or environment [65, 66, 67]. In locomotion, this enables real-time, terrain-aware motions. For instance, DiPPeR [68] conditions a diffusion model on elevation maps to produce feasible 2D paths for quadrupeds, outperforming traditional sampling-based planners in efficiency and generalization. Building on this,

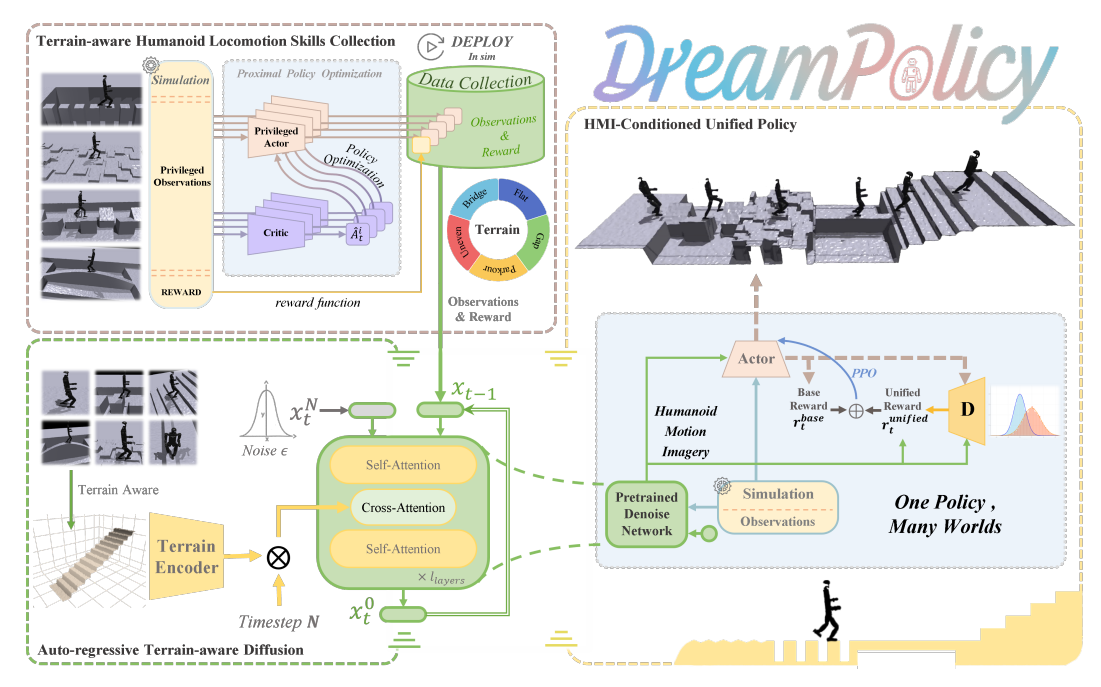


Figure 2: Framework of DreamPolicy. The system is decomposed into two parts: (1) Terrain-aware humanoid locomotion skill data collection, sufficient humanoid locomotion skill data on various challenging terrains will be collected; (2) DreamPolicy, training a unified policy across diverse terrains using skill data and humanoid motion imagery via Auto-Regressive Diffusion Model.

DiffuseLoco [69] demonstrates that a single diffusion model can synthesize diverse skills from offline data. Similarly, BiRoDiff [70] leverages diffusion to unify walking behaviors in bipedal systems, enabling smooth gait transitions and adaptation to unseen slopes. Beyond online planning, diffusion models have also been applied to offline robot learning, where they serve as expressive priors for trajectory optimization or policy distillation [71, 72]. These works collectively highlight diffusion's growing role in scalable, multi-skill locomotion systems, bridging planning, control, and generative modeling.

3 Terrain-aware Humanoid Locomotion Skills Collection

In this section, we will introduce how we collect terrain-aware humanoid locomotion skill data. Section 3.1 describes the data collection framework and benchmarks for evaluating our policy. In section 3.2, we describe how we train specialized policies to obtain primitive skills.

3.1 Humanoid Locomotion Benchmarks with Diverse Terrains

We developed a modular humanoid terrain benchmark to evaluate our method and facilitate skill acquisition comprehensively. This benchmark includes over a dozen specialized terrains (e.g., Gap, Stair, Parkour) for expert policy training and challenging composite terrains (e.g., Gap-Bridge, Wave-Bridge) for testing and evaluation, shown in Figure 3. Thanks to the modular design, terrains can be flexibly combined to generate a wide variety of multi-terrain scenarios. Details of the curriculum design and terrain parameters used in our experiments are provided in the Appendix B.1. Performance is quantitatively measured using metrics such as success rate $R_{\rm succ}$ and completion rate $R_{\rm cmp}$. Leveraging terrain-level design and curriculum learning enables other higher-quality skill acquisition and improved upper-bound performance. An efficient, reusable recording module supports comprehensive data collection in simulation, capturing proprioceptive robot data, external observations (e.g., depth images, radar scans), and reward signals. This facilitates unified policy training, anomaly detection, and targeted fine-tuning. Ultimately, we collected data from six expert policies, yielding a dataset of 75 million samples. As shown in Figures 6 and 5, this expert dataset was crucial to DreamPolicy's strong performance.

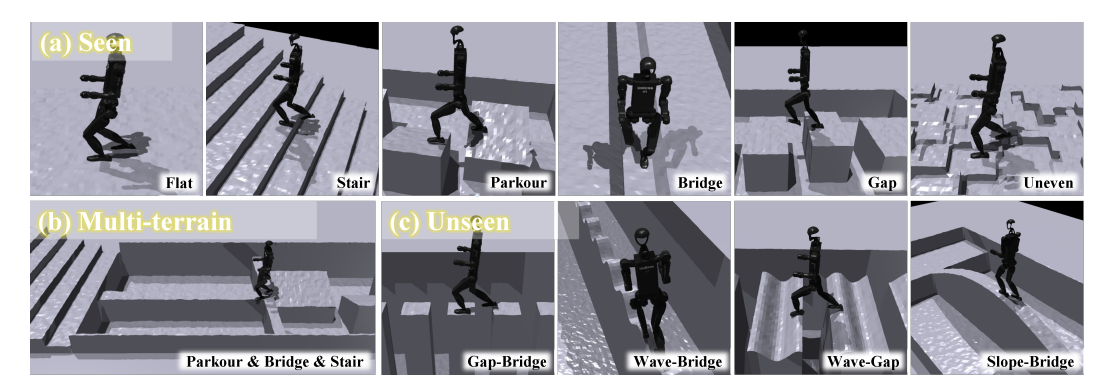


Figure 3: Scenarios visualization. These figures are all the terrain used for evaluation.

3.2 Humanoid Primitive Skills Collection via Specialized Policy Learning

To acquire primitive humanoid robot locomotion skill data, we first train multiple physically feasible policies $\pi = [\pi_1, \pi_2, ..., \pi_n]$ in a large-scale parallel simulator [73] using reinforcement learning, where π_i is an ideal policy trained on single but challenging terrains. Due to the high sampling efficiency of the Proximal Policy Optimization (PPO) algorithm [74] and the parallelized architecture of the simulator, a set of terrain-specific policies is accessible.

Every single policy was specialized for individual terrains and lacked generalization capabilities across diverse scenarios, which will be discussed in section 5.2. Despite environmental variations, all policies share the same network architecture, enabling parameter sharing while training. The observation space and action space will be described later. A single specialized policy adopts a two-phase progressive training: First, a foundational locomotion policy is trained from scratch under a strict regularization penalty, which encourages a basic walk skill without risking early termination due to complex terrain. Second, scenario-specific policies are refined through terrain-specific reward shaping. Inspired by [3], we integrated simulator-generated scandot data (analogous to real-world LiDAR perception) to imbue policies with challenging terrain awareness.

Observation Space and Action Space. The policy observations, which denotes as o_t , consist of:

$$o_t = [o_t^{\text{proprio}}, o_t^{\text{terrain}}, o_t^{\text{hist}}, c_t, a_{t-1}], \tag{1}$$

where o_t^{proprio} , o_t^{terrain} , o_t^{hist} , c_t , a_{t-1} are proprioceptive information, perceptive information, history proprioception, commands, and action of the last timestep. Proprioceptive information is defined as $o_t^{\text{proprio}} = [w_t, g_t, \theta_t, \dot{\theta}_t]$, which contains base angular velocity, orientation data (described as gravity direction in the robot frame), joint position, and joint velocity. Commands consist of the desired velocity $c_t = [v_x, v_y, w_{\text{yaw}}]$, where v_x, v_y, w_{yaw} are the linear velocity of longitudinal and lateral directions, and the angular velocity perpendicular to the ground, respectively. Perceptive information o_t^{terrain} , which is an egocentric height map in the robot's frame, aligning its z-axis to the negative direction of gravity. a_{t-1} is included to provide temporal context. The action $a_t \in \mathbb{R}^{12}$ represents the joint positions for the lower body joints of the humanoid robot. It is noteworthy that only lower-body joints positions $a_t = a_t^{\text{lower}}$ are actively controlled by the actor network, while the upper-body joints a_t^{upper} (irrelevant to locomotion dynamics) are directly assigned default poses to minimize unnecessary computational overhead. More details about the specialized policy learning are provided in the Appendix B.2.

4 DreamPolicy: Unified Policy for Cross-Terrain Humanoid Locomotion

In this section, the detailed implementation of the DreamPolicy framework is illustrated in Figure 2 will be introduced. In section 4.1, we introduce details of Terrain-Aware Diffusion for Humanoid Motion Imagery. In section 4.2, we introduce how we formulate the HMI-conditioned Unified Policy with an AMP-style [75] reward.

4.1 Humanoid Motion Imagery (HMI) via Terrain-Aware Autoregressive Diffusion Planner

Based on large-scale multi-expert locomotion skill data collected in section 3.2, we introduce a terrain-aware autoregressive diffusion model to generate adaptable and scalable humanoid trajectories.

Autoregressive Denoising on State Space. We define the humanoid state s_t at RL timestep t as the concatenation of all joint and root features:

$$s_t = \left[\theta_t, \dot{\theta}_t, p_t, \dot{p}_t, \omega_t, v_t\right],\tag{2}$$

where θ_t , $\dot{\theta}_t$, p_t , \dot{p}_t , ω_t , v_t are joint position, joint velocity, 3D position and rotation on the humanoid, root angular and linear velocities.

Rather than applying diffusion to actions (which are often discrete or vary in dimension), as analysed in [76], we diffuse over the state trajectories. At each control step t, given the history K frames of humanoid state $\mathbf{x}_{t-1} = [s_{t-K+1}, \ldots, s_t]$ and current local terrain embedding $y_t = \mathcal{E}_{\text{terrain}}(o_t^{\text{terrain}})$, The goal is to sample the next H humanoid states $\mathbf{x}_t = [s_{t+1}, \ldots, s_{t+H}]$ conditioned on (x_{t-1}, y_t) .

For generative modeling, we follow a Denoising Diffusion Probabilistic Model (DDPM) [48] framework by gradually adding Gaussian noise to the clean humanoid state trajectory \mathbf{x}_t^0 over N steps. Formally, the forward process for diffusion timestep $n \in \{1, \dots, N\}$ is:

$$q(\mathbf{x}^n|\mathbf{x}^{n-1}) = \mathcal{N}(\sqrt{\alpha_n}\mathbf{x}^{n-1}, (1-\alpha_n)\mathbf{I}),\tag{3}$$

where $\alpha_n \in (0,1)$ are fixed variance-scheduling parameter for step n. In the reverse process, we form the input to the denoiser as $(\mathbf{x}_t^n, \mathbf{x}_{t-1}, n, y_t)$. A transformer-based denoiser \mathcal{G} is trained to predict the cleaned humanoid state trajectory x_t^0 from the noisy input.

$$\hat{\mathbf{x}}_t^0 = \mathcal{G}(\mathbf{x}_t^n, \mathbf{x}_{t-1}, n, y_t), \tag{4}$$

where \hat{x}_t^0 is the model's estimate of the true states. Notably, we predict the states themselves rather than the noise terms, which can improve stability [65]. During training, terrain embedding is randomly masked by a rate of 0.1 for classifier-free guidance sampling at inference[77].

Training. We train on our expert locomotion dataset by minimizing the mean-squared error between the predicted and true states. The diffusion reconstruction loss is:

$$\mathcal{L}_{\text{diffusion}} = \mathbb{E}_{\mathbf{x}^0 \sim q(\mathbf{x}^0), n \sim [1, N]}[\|\mathbf{x}^0_t - \hat{\mathbf{x}}^0_t\|_2^2]. \tag{5}$$

During training, to improve stability and performance, we use a scheduled sampling strategy [78, 79], where the state history is sampled at the probability p from the ground truth or from the model's own previous predictions. We gradually anneal the probability p of using true history from 1 to 0 (from fully teacher-forced to fully autoregressive). This curriculum aligns training and inference behavior, preventing divergence in long sequences.

Inference. After training a denoise network \mathcal{G} , we can auto-regressively generate motion imagery given history states \mathbf{x}_{t-1} , a standard sampler \mathcal{S} like [48, 80] and online terrain embeddings y_t by sampling with classifier-free guidance [77]:

$$\mathcal{G}_{\omega}(\mathbf{x}_{t}^{n}, \mathbf{x}_{t-1}, n, y_{t}) = \mathcal{G}(\mathbf{x}_{t}^{n}, \mathbf{x}_{t-1}, n, \phi) + \omega \cdot \left(\mathcal{G}(\mathbf{x}_{t}^{n}, \mathbf{x}_{t-1}, n, y_{t}) - \mathcal{G}(\mathbf{x}_{t}^{n}, \mathbf{x}_{t-1}, n, \phi)\right), \quad (6)$$

where ω is the guidance hyper-parameter, detailed in Appendix B.3.

4.2 HMI-Conditioned Unified Policy for Cross-Terrain Humanoid Locomotion

HMI-conditioned policy operates as a goal-conditioned reinforcement learning (GCRL) policy, which is mentioned in [81]. Here, the goal $g_t \in \mathbb{R}^{d \times H}$ represents the diffusion-synthesized subgoal trajectory $s_{t+1:t+H}$ generated by terrain-aware autoregressive diffusion planner, with d denoting the state dimension and H the prediction horizon.

Reward Design for HMI-Conditioned Unified Policy. Inspired by [75, 82], we design our HMI-conditioned policy reward for time step t as:

$$r_t = w^{\text{base}} r_t^{\text{base}} + w^{\text{unified}} r_t^{\text{unified}} \tag{7}$$

where r_t^{base} represents basic regularization reward for robot, r_t^{unified} represents unified reward for tracking goal, which has two components: r_t^{goal} encourages goal achievement, r_t^{amp} provides style-based regularization inspired by expert motion manifold modeling [75]. w^{base} , w^{unified} denote weights for these reward terms respectively, w^{unified} contains w^{goal} and w^{amp} . Unlike conventional tracking policies, which typically rely on short-horizon predicted targets, our framework integrates a discriminator reward r_t^{amp} to enable the policy to benefit from both short-term and long-term objectives.

Base Reward for Robotics. The base regularization reward r_t^{base} constrains fundamental robotic behaviors through serveral components. It ensures physically plausible behaviors through regularization on joint positions, velocities, and torques. This includes penalties for excessive joint accelerations, deviations from nominal joint ranges, and abrupt torque changes. Additionally, it encourages smooth base motion and minimal ground contact forces to avoid unnatural oscillations or instability.

Unified Reward for Short-Term. The goal reward $r_t^{\rm goal}$ is designed to guide the policy in closely tracking both the robot's joint positions θ_t and velocities $\dot{\theta}_t$ (in its local coordinate frame), body keypoint position and rotation, as well as the base linear and angular velocities. This ensures naturalistic, stable locomotion. $r_t^{\rm goal}$ is formulated as:

$$r_t^{\text{goal}} = \sum_{i \in \mathcal{Z}} w_i \cdot \exp\left(-\alpha_i \left\| z_{t,i} - \hat{z}_{t,i} \right\|_2\right), \tag{8}$$

where $\mathcal{Z} = \{\theta, \dot{\theta}, p, \dot{p}, \omega, v\}$ is the set of state variables in s_t contributing to the reward, w_i, α_i are the weight coefficient and decay coefficient for variable i.

Unified Reward for Long-Term. The discriminator reward $r_t^{\rm amp}$ is computed by sampling multiple future state sequences from the Terrain-Aware Diffusion Planner within a single timestep. These sequences, conditioned on the robot's history state $s_{t-K:t}$ and terrain context, encapsulate valid locomotion styles that respect terrain-specific dynamics. A discriminator D is jointly trained with the policy and evaluates whether the policy transitions match the "good style" distribution learned from our Terrain-Aware diffusion planner. Following the least-squares loss proposed by AMP[75], the objective of our discriminator is formulated as:

$$\arg\min_{D} \mathbb{E}_{(\hat{s}_{t}, \hat{s}_{t+1}) \sim p_{\text{diff}}} \left[(D(\hat{s}_{t}, \hat{s}_{t+1}) - 1)^{2} \right] + \mathbb{E}_{(s_{t}, s_{t+1}) \sim \pi} \left[(D(s_{t}, s_{t+1}) + 1)^{2} \right], \tag{9}$$

where \hat{s}_t, \hat{s}_{t+1} is state transition sampled from diffusion model, s_t, s_{t+1} is the policy rollouts. As referred to in AMP, the discriminator reward is defined as:

$$r_t^{\text{amp}} = \max\left\{0, 1 - (D(s_t, s_{t+1}) - 1)^2 / 4\right\},\tag{10}$$

which encourages the policy to produce trajectories that align with the diffusion model's implicit knowledge of stable, adaptive locomotion. Compared to standard AMP [75] reward which relies on offline-sampled action sequences from fixed datasets, our method uniquely employs online inference conditioned on the robot's real-time state $s_{t-K+1:t}$ to generate the sequence set $\hat{s}_{t+1:t+H}^{(k)}$. Therefore, a more powerful discriminator is trained on real-time policy trajectories and diffusion-filtered style samples. More details about the HMI-conditioned unified policy are provided in the Appendix B.4.

5 Experiment

In this section, we conduct comprehensive experiments to evaluate the performance of the proposed DreamPolicy method in various scenarios with complex terrains. Specifically, we first depict the setup of our new humanoid locomotion benchmarks with different terrains. Then we compared our method with the previous works in these benchmarks to demonstrate its efficiency. Moreover, ablation analysis on the two components of DreamPolicy and scaling analysis with more trajectory and terrain data are also performed subsequently for a more in-depth exploration of DreamPolicy.

5.1 Experimental Setup

Comparison Methods. We compare our method against the following settings: 1) a Vanilla Actor-Critic approach (rsl_rl [83]) with specialized reward functions; 2) a Scenario Specialized Policy that extends the Actor-Critic architecture with a Scandot encoder and privileged estimator module; 3) a

distillation-based method following approaches such as DAgger [84] [85]; 4) an ablation without the Diffusion Planner and 5) an ablation without HMI-conditioned RL (we called GCRL). More design details are provided in the Appendix C.1.

Scenarios. All training and simulations are conducted in IsaacGym [73]. We evaluated our method on 1) selected typical six single-terrains (*Flat, Gap, Stair, Bridge, Parkour, Uneven*). 2) Four multiterrains stages from stage 1 (*parkour & stair*) to stage 4 (*parkour & stair & bridge & uneven & gap*). 3) Four unseen terrains (*Gap-bridge, Slope-bridge, Wave-bridge, Wave-gap*). As shown in Figure 3. To undulate the ground, we add base roughness for all terrains. Notably, prior research typically used test terrains longer than 4m [2] and 8m [25] for single terrains and 4.8m [9] per segment in multi-terrain settings. To ensure a more robust evaluation and minimize random effects, we increase the single terrain length to 18m and set each multi-terrain segment to 9m. More design details are provided in the Appendix B.1

Metrics. We evaluated all settings using the following metrics. 1) Success Rate R_{succ} : The percentage of successful attempts to cross the entire terrain. 2) Complete Rate R_{cmp} : The ratio of the distance traveled before falling to the total terrain length.

5.2 Performance Comparison on Different Terrains

Single-terrain. We evaluated the performance of each setting on a single-terrain, the results are shown in Figure 4. Our method maintains a comparable completion rate to expert policies on single terrains, even when learning across multiple terrains. Additionally, unlike specialized distillation methods, our approach does not exhibit significant performance degradation, indicating that the diffusion model possesses strong recovery capabilities.

Table 1: **Performance Comparison in Multi-terrain scenarios.** All data in the table are shown as percentages, the higher the better. From Stage 1 to Stage 4, we gradually add single terrain from (*Parkour & Stair*) to (*Rarkour & Stair & Bridge & Uneven & Gap*). The best results are highlighted in boldface.

	Parkour&Stair		Stage 1	+Bridge	Stage 2-	-Uneven	Stage 3+Gap	
	$R_{\rm succ}(\%)$	$R_{\rm cmp}(\%)$						
Vanilla [83]	0.00 ± 0.00	$5.22{\scriptstyle\pm0.56}$	0.00 ± 0.00	$5.48{\scriptstyle\pm0.59}$	0.00 ± 0.00	$5.36{\scriptstyle\pm0.42}$	0.00 ± 0.00	5.11 ± 0.46
Distillation [84]	$51.33{\scriptstyle\pm0.19}$	$88.34{\scriptstyle\pm0.21}$	$48.05{\scriptstyle\pm0.12}$	$81.46{\scriptstyle\pm0.34}$	$26.84{\scriptstyle\pm0.75}$	$62.66{\scriptstyle\pm0.87}$	$21.22{\scriptstyle\pm0.97}$	$51.52{\scriptstyle\pm1.14}$
Ours	$\textbf{70.38} {\pm} 0.02$	$92.33 {\pm} 0.08$	$\textbf{67.16} {\pm} 0.01$	89.34 ±0.09	$\textbf{58.11} {\pm} 0.05$	$\pmb{80.21} {\pm} 0.14$	$\textbf{56.14} {\pm} 0.06$	76.34 ±0.27
Ours w/o Diffusion	32.26 ± 0.28	74.36 ± 0.66	30.15 ± 0.36	$65.32{\pm}0.78$	17.16 ± 0.82	44.28 ± 1.47	16.34 ± 0.88	39.48 ± 1.15
Ours w/o GCRL	$0.00\pm$ 0.00	$1.57{\scriptstyle\pm0.19}$	0.00 ± 0.00	$1.16{\scriptstyle\pm0.22}$	0.00 ± 0.00	$1.22{\scriptstyle\pm0.39}$	0.00 ± 0.00	1.35 ± 0.17

Multi-terrains. To evaluate the generalization ability of each setting across different scenarios, we test all methods in multi-terrain environments. Across all terrain types, it consistently outperforms other approaches, shown in Table 1. As the diversity and complexity of terrains increase, our method maintains consistently high performance without substantial degradation. This shows that our generalization performance is relatively stable. Notably, our method also exhibits low variance across multiple trials, indicating strong robustness.

Unseen terrains. To assess the zero-shot capabilities of each method on complex terrains, we evaluated all settings on four challenging unseen environments. On challenging terrains, our method demonstrates superior generalization compared to other approaches, as shown in Table 2. Notably, on



Figure 4: Comparison in Single terrain

Table 2: **Performance Comparison in Unseen-terrain scenarios.** All data in the table are shown as percentages, the higher the better. The best results are highlighted in boldface.

	Gap-Bridge		Slope-	Bridge	Wave	-Gap	Wave-Bridge	
	$R_{\rm succ}(\%)$	$R_{\rm cmp}(\%)$	$R_{\rm succ}(\%)$	$R_{\rm cmp}(\%)$	$R_{ m succ}(\%)$	$R_{\rm cmp}(\%)$	$\overline{R_{ m succ}(\%)}$	$R_{\rm cmp}(\%)$
Vanilla [83]	0.08 ± 0.00	$7.35{\scriptstyle\pm2.74}$	$0.35{\pm}1.37$	$17.14{\scriptstyle\pm0.77}$	0.00 ± 0.00	$3.72{\scriptstyle\pm0.14}$	0.00 ± 0.00	$6.15{\scriptstyle\pm0.08}$
Distillation [84]	$11.26{\scriptstyle\pm1.25}$	$38.03{\scriptstyle\pm4.72}$	$31.05{\scriptstyle\pm5.82}$	$55.88{\scriptstyle\pm2.36}$	$25.36{\scriptstyle\pm2.58}$	$38.76{\scriptstyle\pm1.55}$	0.00 ± 0.00	$15.34{\scriptstyle\pm6.25}$
Ours	$31.33 {\pm} 0.07$	$64.25 {\pm} 0.23$	$\textbf{72.56} {\pm} 0.13$	$\textbf{78.34} {\pm} 0.28$	$\textbf{45.18} {\pm} 0.14$	$58.26 {\pm} 0.48$	8.25 ± 0.14	37.77 ±0.45
Ours w/o Diffusion	8.23 ± 0.01	21.04 ± 0.16	15.78 ± 0.22	20.27 ± 0.16	0.01 ± 0.01	$15.25{\scriptstyle\pm3.39}$	0.00 ± 0.00	$5.25{\scriptstyle\pm1.22}$
Ours w/o GCRL	$0.01{\scriptstyle\pm0.01}$	$2.77{\pm}0.84$	$0.00{\pm}0.00$	$5.34{\scriptstyle\pm2.18}$	0.00 ± 0.00	$3.47{\scriptstyle\pm0.14}$	$0.00{\pm}0.00$	$2.58{\scriptstyle\pm0.04}$

the *Wave-Bridge* terrain, our method is able to achieve task completion, albeit with a lower success rate, while other methods fail to succeed entirely.

Above all, our method demonstrates strong generalization, as well as exceptional stability and robustness. More experimental results are provided in the Appendix C.2.

5.3 Ablation Analysis

To further explore the contribution of each component in our algorithm to the performance, we conduct an ablation study on DreamPolicy without the diffusion planner and goal-conditioned RL.

DreamPolicy w./w.o. Diffusion Planner. DreamPolicy ablation experiments without the diffusion planner indicate that relying only on offline expert data leads to suboptimal and rapidly worsening performance as terrain complexity increases (see Table 1 and 2). This is because, when encountering out-of-distribution (OOD) states or complex observations, the model cannot draw effective guidance from experience, which can even negatively impact training. Additionally, removing the diffusion planner improves inference speed by approximately 100ms, indicating its impact on overall efficiency.

DreamPolicy w./w.o. GCRL. Ablation results without HMI-conditioned RL indicate that relying solely on the diffusion planner performs well on simple terrains (Figure 4) but fails on more complex environments (Table 1 and 2). While the diffusion planner can generate optimal policies, these are not always physically feasible and can be disrupted by environmental factors, such as stumbling on uneven ground. Notably, BiRoDiff [70], which uses a similar architecture, exhibits consistent results, further supporting our findings.

5.4 Scaling Analysis

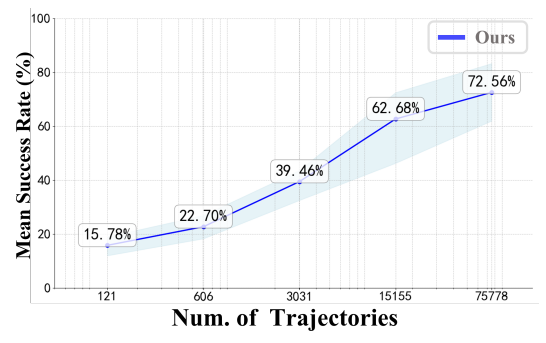


Figure 5: Success rate on Slope-Bridge with expert dataset scales.

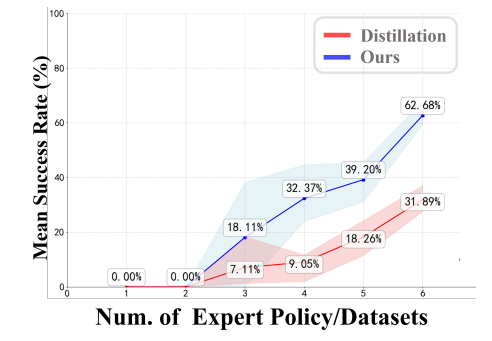


Figure 6: Success rate on Slope-Bridge with expert dataset types.

Besides, we also conduct experiments on the unseen terrain (Gap-bridge) to show the scaling-up ability of our DreamPolicy compared with the Distillation method.

Scaling Capability with the Number of Trajectories Learned. To evaluate the impact of dataset size, we divided our offline dataset into subsets ranging from 120K to 75M samples and measured the diffusion model's planning success rate (Figure 5). Results show that larger datasets significantly boost planning performance, highlighting the model's ability to leverage large-scale data.

Scaling Capability with the Number of Terrains Learned. We evaluated our model by training expert policies on combinations of one to six terrains. As shown in Figure 6, increasing the number of expert terrain types steadily improves generalization, with each new terrain type enhancing overall performance. Compared to a distillation-based model such as DAgger, our method consistently achieves higher success rates, while DAgger requires more terrain variety to perform reasonably and still underperforms.

6 Conclusion, Limitations and Future Works

We propose **DreamPolicy**, a unified framework enabling versatile humanoid locomotion across cross-scenario and unseen terrains. DreamPolicy collects expert demonstration data via parallel simulations in varied environments (e.g., stairs, uneven ground). A terrain-aware autoregressive diffusion model is then trained on this data to generate cross-scenario Humanoid Motion Imagery (HMI), capturing rich, multimodal motion patterns. Finally, a physics-constrained, HMI-conditioned policy is optimized, ensuring dynamical feasibility and robust exploration. By combining skill acquisition, motion prior modeling, and physics-aware refinement, DreamPolicy achieves broader state—action coverage and superior generalization compared to deterministic RL. While the diffusion-based planner incurs some computational overhead due to iterative denoising, future work will explore lightweight samplers to accelerate inference without sacrificing trajectory quality.

Acknowledgement

This work was supported by National Natural Science Foundation of China (62406195, 62303319), Shanghai Local College Capacity Building Program (23010503100), Shanghai Tech AI4S Initiative SHTAI4S202404, HPC Platform of Shanghai Tech University, and MoE Key Laboratory of Intelligent Perception and Human-Machine Collaboration (Shanghai Tech University), and Shanghai Engineering Research Center of Intelligent Vision and Imaging.

References

- [1] Miomir Vukobratović and Juri Stepanenko. On the stability of anthropomorphic systems. *Mathematical biosciences*, 15(1-2):1–37, 1972.
- [2] Weiji Xie, Chenjia Bai, Jiyuan Shi, Junkai Yang, Yunfei Ge, Weinan Zhang, and Xuelong Li. Humanoid whole-body locomotion on narrow terrain via dynamic balance and reinforcement learning. *arXiv preprint arXiv*:2502.17219, 2025.
- [3] Xuxin Cheng, Kexin Shi, Ananye Agarwal, and Deepak Pathak. Extreme parkour with legged robots. In 2024 IEEE International Conference on Robotics and Automation (ICRA), pages 11443–11450. IEEE, 2024.
- [4] Ziwen Zhuang, Zipeng Fu, Jianren Wang, Christopher Atkeson, Soeren Schwertfeger, Chelsea Finn, and Hang Zhao. Robot parkour learning. *arXiv preprint arXiv:2309.05665*, 2023.
- [5] Fatemeh Zargarbashi, Jin Cheng, Dongho Kang, Robert Sumner, and Stelian Coros. Robotkeyframing: Learning locomotion with high-level objectives via mixture of dense and sparse rewards. *arXiv preprint arXiv:2407.11562*, 2024.
- [6] Zipeng Fu, Ashish Kumar, Jitendra Malik, and Deepak Pathak. Minimizing energy consumption leads to the emergence of gaits in legged robots. In *Conference on Robot Learning (CoRL)*, 2021.
- [7] Zipeng Fu, Xuxin Cheng, and Deepak Pathak. Deep whole-body control: Learning a unified policy for manipulation and locomotion. In *Conference on Robot Learning (CoRL)*, 2022.
- [8] Minghuan Liu, Zixuan Chen, Xuxin Cheng, Yandong Ji, Rizhao Qiu, Ruihan Yang, and Xiaolong Wang. Visual whole-body control for legged loco-manipulation. *The 8th Conference on Robot Learning*, 2024.

- [9] Ziwen Zhuang, Shenzhe Yao, and Hang Zhao. Humanoid parkour learning. In 8th Annual Conference on Robot Learning, 2024. URL https://openreview.net/forum?id=fs7ia3FqUM.
- [10] Ilija Radosavovic, Sarthak Kamat, Trevor Darrell, and Jitendra Malik. Learning humanoid locomotion over challenging terrain. *arXiv preprint arXiv:2410.03654*, 2024.
- [11] Ilija Radosavovic, Bike Zhang, Baifeng Shi, Jathushan Rajasegaran, Sarthak Kamat, Trevor Darrell, Koushil Sreenath, and Jitendra Malik. Humanoid locomotion as next token prediction. In *The Thirty-eighth Annual Conference on Neural Information Processing Systems*, 2024.
- [12] Jingxiao Chen, Xinyao Li, Jiahang Cao, Zhengbang Zhu, Wentao Dong, Minghuan Liu, Ying Wen, Yong Yu, Liqing Zhang, and Weinan Zhang. Rhino: Learning real-time humanoid-human-object interaction from human demonstrations. *arXiv preprint arXiv:2502.13134*, 2025.
- [13] Zhaoyuan Gu, Junheng Li, Wenlan Shen, Wenhao Yu, Zhaoming Xie, Stephen McCrory, Xianyi Cheng, Abdulaziz Shamsah, Robert Griffin, C Karen Liu, et al. Humanoid locomotion and manipulation: Current progress and challenges in control, planning, and learning. *arXiv* preprint *arXiv*:2501.02116, 2025.
- [14] Xuxin Cheng, Jialong Li, Shiqi Yang, Ge Yang, and Xiaolong Wang. Open-television: Teleoperation with immersive active visual feedback. *arXiv preprint arXiv:2407.01512*, 2024.
- [15] Xuxin Cheng, Yandong Ji, Junming Chen, Ruihan Yang, Ge Yang, and Xiaolong Wang. Expressive whole-body control for humanoid robots. *arXiv preprint arXiv:2402.16796*, 2024.
- [16] Zipeng Fu, Qingqing Zhao, Qi Wu, Gordon Wetzstein, and Chelsea Finn. Humanplus: Humanoid shadowing and imitation from humans. *arXiv* preprint arXiv:2406.10454, 2024.
- [17] Tairan He, Wenli Xiao, Toru Lin, Zhengyi Luo, Zhenjia Xu, Zhenyu Jiang, Changliu Liu, Guanya Shi, Xiaolong Wang, Linxi Fan, and Yuke Zhu. Hover: Versatile neural whole-body controller for humanoid robots. *arXiv preprint arXiv:2410.21229*, 2024.
- [18] Yufei Xue, Wentao Dong, Minghuan Liu, Weinan Zhang, and Jiangmiao Pang. A unified and general humanoid whole-body controller for fine-grained locomotion. In *Robotics: Science and Systems (RSS)*, 2025.
- [19] Xianqi Zhang, Hongliang Wei, Wenrui Wang, Xingtao Wang, Xiaopeng Fan, and Debin Zhao. Flam: Foundation model-based body stabilization for humanoid locomotion and manipulation. *arXiv preprint arXiv:2503.22249*, 2025.
- [20] Mert Albaba, Chenhao Li, Markos Diomataris, Omid Taheri, Andreas Krause, and Michael Black. Nil: No-data imitation learning by leveraging pre-trained video diffusion models. arXiv preprint arXiv:2503.10626, 2025.
- [21] Qiang Zhang, Peter Cui, David Yan, Jingkai Sun, Yiqun Duan, Gang Han, Wen Zhao, Weining Zhang, Yijie Guo, Arthur Zhang, et al. Whole-body humanoid robot locomotion with human reference. In 2024 IEEE/RSJ International Conference on Intelligent Robots and Systems (IROS), pages 11225–11231. IEEE, 2024.
- [22] Tairan He, Zhengyi Luo, Wenli Xiao, Chong Zhang, Kris Kitani, Changliu Liu, and Guanya Shi. Learning human-to-humanoid real-time whole-body teleoperation. In 2024 IEEE/RSJ International Conference on Intelligent Robots and Systems (IROS), pages 8944–8951. IEEE, 2024.
- [23] Zhenyu Jiang, Yuqi Xie, Jinhan Li, Ye Yuan, Yifeng Zhu, and Yuke Zhu. Harmon: Whole-body motion generation of humanoid robots from language descriptions. *arXiv* preprint *arXiv*:2410.12773, 2024.
- [24] Fabian Jenelten, Jemin Hwangbo, Fabian Tresoldi, C Dario Bellicoso, and Marco Hutter. Dynamic locomotion on slippery ground. *IEEE Robotics and Automation Letters*, 4(4):4170–4176, 2019.

- [25] Huayi Wang, Zirui Wang, Junli Ren, Qingwei Ben, Tao Huang, Weinan Zhang, and Jiangmiao Pang. BeamDojo: Learning agile humanoid locomotion on sparse footholds. In *Robotics: Science and Systems (RSS)*, 2025.
- [26] Junli Ren, Tao Huang, Huayi Wang, Zirui Wang, Qingwei Ben, Jiangmiao Pang, and Ping Luo. Vb-com: Learning vision-blind composite humanoid locomotion against deficient perception. arXiv preprint arXiv:2502.14814, 2025.
- [27] Xinyang Gu, Yen-Jen Wang, Xiang Zhu, Chengming Shi, Yanjiang Guo, Yichen Liu, and Jianyu Chen. Advancing humanoid locomotion: Mastering challenging terrains with denoising world model learning. *arXiv preprint arXiv:2408.14472*, 2024.
- [28] Junfeng Long, Junli Ren, Moji Shi, Zirui Wang, Tao Huang, Ping Luo, and Jiangmiao Pang. Learning humanoid locomotion with perceptive internal model, 2024. URL https://arxiv.org/abs/2411.14386.
- [29] Qiang Zhang, Gang Han, Jingkai Sun, Wen Zhao, Chenghao Sun, Jiahang Cao, Jiaxu Wang, Yijie Guo, and Renjing Xu. Distillation-ppo: A novel two-stage reinforcement learning framework for humanoid robot perceptive locomotion. *arXiv preprint arXiv:2503.08299*, 2025.
- [30] Wandong Sun, Baoshi Cao, Long Chen, Yongbo Su, Yang Liu, Zongwu Xie, and Hong Liu. Learning perceptive humanoid locomotion over challenging terrain. arXiv preprint arXiv:2503.00692, 2025.
- [31] Fangcheng Jin, Yuqi Wang, Peixin Ma, Guodong Yang, Pan Zhao, En Li, and Zhengtao Zhang. Teacher motion priors: Enhancing robot locomotion over challenging terrain. *arXiv preprint arXiv:2504.10390*, 2025.
- [32] Tairan He, Zhengyi Luo, Xialin He, Wenli Xiao, Chong Zhang, Weinan Zhang, Kris Kitani, Changliu Liu, and Guanya Shi. Omnih2o: Universal and dexterous human-to-humanoid whole-body teleoperation and learning. *arXiv preprint arXiv:2406.08858*, 2024.
- [33] Naureen Mahmood, Nima Ghorbani, Nikolaus F Troje, Gerard Pons-Moll, and Michael J Black. Amass: Archive of motion capture as surface shapes. In *Proceedings of the IEEE/CVF international conference on computer vision*, pages 5442–5451, 2019.
- [34] Lingfan Bao, Joseph Humphreys, Tianhu Peng, and Chengxu Zhou. Deep reinforcement learning for bipedal locomotion: A brief survey. *arXiv preprint arXiv:2404.17070*, 2024.
- [35] Ria Doshi, Homer Walke, Oier Mees, Sudeep Dasari, and Sergey Levine. Scaling cross-embodied learning: One policy for manipulation, navigation, locomotion and aviation. *arXiv* preprint arXiv:2408.11812, 2024.
- [36] Yang Hu and Giovanni Montana. Skill transfer in deep reinforcement learning under morphological heterogeneity. *arXiv preprint arXiv:1908.05265*, 2019.
- [37] Devendra Singh Chaplot, Guillaume Lample, Kanthashree Mysore Sathyendra, and Ruslan Salakhutdinov. Transfer deep reinforcement learning in 3d environments: An empirical study. In NIPS deep reinforcemente leaning workshop, volume 138, 2016.
- [38] Wenlong Huang, Igor Mordatch, and Deepak Pathak. One policy to control them all: Shared modular policies for agent-agnostic control. In *International Conference on Machine Learning*, pages 4455–4464. PMLR, 2020.
- [39] Bo Ai, Liu Dai, Nico Bohlinger, Dichen Li, Tongzhou Mu, Zhanxin Wu, K. Fay, Henrik I. Christensen, Jan Peters, and Hao Su. Towards embodiment scaling laws in robot locomotion, 2025. URL https://arxiv.org/abs/2505.05753.
- [40] Nico Bohlinger, Grzegorz Czechmanowski, Maciej Krupka, Piotr Kicki, Krzysztof Walas, Jan Peters, and Davide Tateo. One policy to run them all: an end-to-end learning approach to multi-embodiment locomotion. *arXiv* preprint arXiv:2409.06366, 2024.
- [41] Austin Patel and Shuran Song. Get-zero: Graph embodiment transformer for zero-shot embodiment generalization. *arXiv preprint arXiv:2407.15002*, 2024.

- [42] Gilbert Feng, Hongbo Zhang, Zhongyu Li, Xue Bin Peng, Bhuvan Basireddy, Linzhu Yue, Zhitao Song, Lizhi Yang, Yunhui Liu, Koushil Sreenath, et al. Genloco: Generalized locomotion controllers for quadrupedal robots. In *Conference on Robot Learning*, pages 1893–1903. PMLR, 2023.
- [43] Octo Model Team, Dibya Ghosh, Homer Walke, Karl Pertsch, Kevin Black, Oier Mees, Sudeep Dasari, Joey Hejna, Tobias Kreiman, Charles Xu, et al. Octo: An open-source generalist robot policy. *arXiv preprint arXiv:2405.12213*, 2024.
- [44] Johan Bjorck, Fernando Castañeda, Nikita Cherniadev, Xingye Da, Runyu Ding, Linxi Fan, Yu Fang, Dieter Fox, Fengyuan Hu, Spencer Huang, et al. Gr00t n1: An open foundation model for generalist humanoid robots. *arXiv preprint arXiv:2503.14734*, 2025.
- [45] Anthony Brohan, Noah Brown, Justice Carbajal, Yevgen Chebotar, Joseph Dabis, Chelsea Finn, Keerthana Gopalakrishnan, Karol Hausman, Alex Herzog, Jasmine Hsu, et al. Rt-1: Robotics transformer for real-world control at scale. *arXiv preprint arXiv:2212.06817*, 2022.
- [46] Anthony Brohan, Noah Brown, Justice Carbajal, Yevgen Chebotar, Xi Chen, Krzysztof Choromanski, Tianli Ding, Danny Driess, Avinava Dubey, Chelsea Finn, et al. Rt-2: Vision-language-action models transfer web knowledge to robotic control. arXiv preprint arXiv:2307.15818, 2023.
- [47] Yang Song, Jascha Sohl-Dickstein, Diederik P Kingma, Abhishek Kumar, Stefano Ermon, and Ben Poole. Score-based generative modeling through stochastic differential equations. *arXiv* preprint arXiv:2011.13456, 2020.
- [48] Jonathan Ho, Ajay Jain, and Pieter Abbeel. Denoising diffusion probabilistic models. *Advances in neural information processing systems*, 33:6840–6851, 2020.
- [49] Prafulla Dhariwal and Alexander Nichol. Diffusion models beat gans on image synthesis. *Advances in neural information processing systems*, 34:8780–8794, 2021.
- [50] Jonathan Ho, Tim Salimans, Alexey Gritsenko, William Chan, Mohammad Norouzi, and David J Fleet. Video diffusion models. *Advances in Neural Information Processing Systems*, 35:8633–8646, 2022.
- [51] Andreas Blattmann, Robin Rombach, Huan Ling, Tim Dockhorn, Seung Wook Kim, Sanja Fidler, and Karsten Kreis. Align your latents: High-resolution video synthesis with latent diffusion models. In *Proceedings of the IEEE/CVF conference on computer vision and pattern recognition*, pages 22563–22575, 2023.
- [52] Cheng Chi, Zhenjia Xu, Siyuan Feng, Eric Cousineau, Yilun Du, Benjamin Burchfiel, Russ Tedrake, and Shuran Song. Diffusion policy: Visuomotor policy learning via action diffusion. *The International Journal of Robotics Research*, page 02783649241273668, 2023.
- [53] Yanjie Ze, Gu Zhang, Kangning Zhang, Chenyuan Hu, Muhan Wang, and Huazhe Xu. 3d diffusion policy: Generalizable visuomotor policy learning via simple 3d representations. In *Proceedings of Robotics: Science and Systems (RSS)*, 2024.
- [54] Michael Janner, Yilun Du, Joshua Tenenbaum, and Sergey Levine. Planning with diffusion for flexible behavior synthesis. In *International Conference on Machine Learning*, pages 9902–9915. PMLR, 2022.
- [55] Shijie Wu, Yihang Zhu, Yunao Huang, Kaizhen Zhu, Jiayuan Gu, Jingyi Yu, Ye Shi, and Jingya Wang. AffordDP: Generalizable diffusion policy with transferable affordance. arXiv preprint arXiv:2412.03142, 2024.
- [56] Zhendong Wang, Jonathan J Hunt, and Mingyuan Zhou. Diffusion policies as an expressive policy class for offline reinforcement learning. In *The Eleventh International Conference on Learning Representations*, 2023.
- [57] Bingyi Kang, Xiao Ma, Chao Du, Tianyu Pang, and Shuicheng Yan. Efficient diffusion policies for offline reinforcement learning. Advances in Neural Information Processing Systems, 36: 67195–67212, 2023.

- [58] Liyuan Mao, Haoran Xu, Xianyuan Zhan, Weinan Zhang, and Amy Zhang. Diffusion-dice: In-sample diffusion guidance for offline reinforcement learning. In *The Thirty-eighth Annual Conference on Neural Information Processing Systems*, 2024.
- [59] Long Yang, Zhixiong Huang, Fenghao Lei, Yucun Zhong, Yiming Yang, Cong Fang, Shiting Wen, Binbin Zhou, and Zhouchen Lin. Policy representation via diffusion probability model for reinforcement learning. arXiv preprint arXiv:2305.13122, 2023.
- [60] Michael Psenka, Alejandro Escontrela, Pieter Abbeel, and Yi Ma. Learning a diffusion model policy from rewards via q-score matching. In *International Conference on Machine Learning*, pages 41163–41182. PMLR, 2024.
- [61] Shutong Ding, Ke Hu, Zhenhao Zhang, Kan Ren, Weinan Zhang, Jingyi Yu, Jingya Wang, and Ye Shi. Diffusion-based reinforcement learning via q-weighted variational policy optimization. In *The Thirty-eighth Annual Conference on Neural Information Processing Systems*, 2024.
- [62] Junjie Wen, Minjie Zhu, Yichen Zhu, Zhibin Tang, Jinming Li, Zhongyi Zhou, Chengmeng Li, Xiaoyu Liu, Yaxin Peng, Chaomin Shen, et al. Diffusion-vla: Scaling robot foundation models via unified diffusion and autoregression. *arXiv preprint arXiv:2412.03293*, 2024.
- [63] Yuhui Chen, Haoran Li, and Dongbin Zhao. Boosting continuous control with consistency policy. In *Proceedings of the 23rd International Conference on Autonomous Agents and Multiagent Systems*, pages 335–344, 2024.
- [64] Jiaming Liu, Hao Chen, Pengju An, Zhuoyang Liu, Renrui Zhang, Chenyang Gu, Xiaoqi Li, Ziyu Guo, Sixiang Chen, Mengzhen Liu, et al. Hybridvla: Collaborative diffusion and autoregression in a unified vision-language-action model. arXiv preprint arXiv:2503.10631, 2025.
- [65] Guy Tevet, Sigal Raab, Setareh Cohan, Daniele Reda, Zhengyi Luo, Xue Bin Peng, Amit H Bermano, and Michiel van de Panne. CLoSD: Closing the loop between simulation and diffusion for multi-task character control. *arXiv preprint arXiv:2410.03441*, 2024.
- [66] Kaifeng Zhao, Gen Li, and Siyu Tang. Dartcontrol: A diffusion-based autoregressive motion model for real-time text-driven motion control. In *The Thirteenth International Conference on Learning Representations*, 2024.
- [67] Joao Carvalho, An T Le, Mark Baierl, Dorothea Koert, and Jan Peters. Motion planning diffusion: Learning and planning of robot motions with diffusion models. In 2023 IEEE/RSJ International Conference on Intelligent Robots and Systems (IROS), pages 1916–1923. IEEE, 2023.
- [68] Jianwei Liu, Maria Stamatopoulou, and Dimitrios Kanoulas. Dipper: Diffusion-based 2d path planner applied on legged robots. In 2024 IEEE International Conference on Robotics and Automation (ICRA), pages 9264–9270. IEEE, 2024.
- [69] Xiaoyu Huang, Yufeng Chi, Ruofeng Wang, Zhongyu Li, Xue Bin Peng, Sophia Shao, Borivoje Nikolic, and Koushil Sreenath. DiffuseLoco: Real-time legged locomotion control with diffusion from offline datasets. In 8th Annual Conference on Robot Learning, 2024.
- [70] GVS Mothish, Manan Tayal, and Shishir Kolathaya. Birodiff: Diffusion policies for bipedal robot locomotion on unseen terrains. *arXiv preprint arXiv:2407.05424*, 2024.
- [71] Wanming Yu, Fernando Acero, Vassil Atanassov, Chuanyu Yang, Ioannis Havoutis, Dimitrios Kanoulas, and Zhibin Li. Discovery of skill switching criteria for learning agile quadruped locomotion. arXiv preprint arXiv:2502.06676, 2025.
- [72] Xinyi Yuan, Zhiwei Shang, Zifan Wang, Chenkai Wang, Zhao Shan, Meixin Zhu, Chenjia Bai, Xuelong Li, Weiwei Wan, and Kensuke Harada. Preference aligned diffusion planner for quadrupedal locomotion control. *arXiv preprint arXiv:2410.13586*, 2024.
- [73] Viktor Makoviychuk, Lukasz Wawrzyniak, Yunrong Guo, Michelle Lu, Kier Storey, Miles Macklin, David Hoeller, Nikita Rudin, Arthur Allshire, Ankur Handa, et al. Isaac gym: High performance gpu-based physics simulation for robot learning. arXiv preprint arXiv:2108.10470, 2021.

- [74] John Schulman, Filip Wolski, Prafulla Dhariwal, Alec Radford, and Oleg Klimov. Proximal policy optimization algorithms. *arXiv* preprint arXiv:1707.06347, 2017.
- [75] Xue Bin Peng, Ze Ma, Pieter Abbeel, Sergey Levine, and Angjoo Kanazawa. Amp: Adversarial motion priors for stylized physics-based character control. *ACM Transactions on Graphics* (*ToG*), 40(4):1–20, 2021.
- [76] Anurag Ajay, Yilun Du, Abhi Gupta, Joshua Tenenbaum, Tommi Jaakkola, and Pulkit Agrawal. Is conditional generative modeling all you need for decision-making? *arXiv* preprint *arXiv*:2211.15657, 2022.
- [77] Jonathan Ho and Tim Salimans. Classifier-free diffusion guidance. In *NeurIPS 2021 Workshop on Deep Generative Models and Downstream Applications*, 2021.
- [78] Samy Bengio, Oriol Vinyals, Navdeep Jaitly, and Noam Shazeer. Scheduled sampling for sequence prediction with recurrent neural networks. *Advances in neural information processing systems*, 28, 2015.
- [79] Ye Yuan, Viktor Makoviychuk, Y Guo, S Fidler, XB Peng, and K Fatahalian. Learning physically simulated tennis skills from broadcast videos. ACM Trans. Graph, 42(4), 2023.
- [80] Jiaming Song, Chenlin Meng, and Stefano Ermon. Denoising diffusion implicit models. arXiv preprint arXiv:2010.02502, 2020.
- [81] Minghuan Liu, Menghui Zhu, and Weinan Zhang. Goal-conditioned reinforcement learning: Problems and solutions. *arXiv preprint arXiv:2201.08299*, 2022.
- [82] Zhengyi Luo, Jinkun Cao, Kris Kitani, Weipeng Xu, et al. Perpetual humanoid control for real-time simulated avatars. In *Proceedings of the IEEE/CVF International Conference on Computer Vision*, pages 10895–10904, 2023.
- [83] Nikita Rudin, David Hoeller, Philipp Reist, and Marco Hutter. Learning to walk in minutes using massively parallel deep reinforcement learning. In *Conference on Robot Learning*, pages 91–100. PMLR, 2022.
- [84] Dian Chen, Brady Zhou, Vladlen Koltun, and Philipp Krähenbühl. Learning by cheating. In *Conference on robot learning*, pages 66–75. PMLR, 2020.
- [85] Stéphane Ross, Geoffrey Gordon, and Drew Bagnell. A reduction of imitation learning and structured prediction to no-regret online learning. In *Proceedings of the fourteenth international conference on artificial intelligence and statistics*, pages 627–635. JMLR Workshop and Conference Proceedings, 2011.

One Policy but Many Worlds: A Scalable Unified Policy for Versatile Humanoid Locomotion

Supplementary Material

Appendix

A	Ove	rview	16
В	Sup	plementary Technical Details	16
	B.1	Details of Humanoid Locomotion Benchmarks	16
	B.2	Details of Specialized Policy Learning	17
	B.3	Details of Autoregressive Diffusion Planner	18
	B.4	Details of HMI-conditioned Unified Policy	20
C	Add	itional Experiments and Results	21
	C.1	Detailed Implementation of Baselines	21
	C.2	Additional Experiments	22
	C.3	Additional Visualization Results	22
D	Sup	plementary Video	23
E	Exte	ended Limitation and Discussions	24
	E.1	Limitation and Failure Cases	24
	E.2	Discussion and Future Work	24

A Overview

The appendix provides comprehensive supplementary materials supporting the methodological and empirical contributions of this work. Section B elaborates on technical implementations, including the configuration of humanoid locomotion benchmarks (B.1), specialized policy training protocols (B.2), architectural details of the autoregressive diffusion planner (B.3), and the design principles of the HMI-conditioned unified policy (B.4). Section C presents extended experimental analyses, encompassing baseline implementation specifics (C.1), additional performance evaluations across diverse scenarios (C.2), qualitative visualizations (C.3), and supplementary video demonstrations (D). Section E concludes with an in-depth discussion of limitations through failure case examinations (E.1) and potential future research directions (E.2).

B Supplementary Technical Details

B.1 Details of Humanoid Locomotion Benchmarks

Curriculum design For the parameters in the table, p[0] represents the first dimension, p[1] represents the second dimension. If p[0] > p[1], the larger the parameter, the simpler it is. The curriculum design is as follows:

$$\label{eq:truth_parameters} \text{Truth parameters} = \text{random}\left(\frac{(p[1]-p[0])}{\text{max_terrain_level}} \times \text{Difficulty}\right) + p[0]$$

Detailed parameters of different terrains. For all terrains, we add base roughness to make the ground undulating. The height of the ground is between height = random(-0.05, 0.05) * difficulty. Difficulty increases with the terrain level. To ensure a more robust evaluation and minimize random effects, we increase the single terrain length to 18m and set each multi-terrain segment to 9m.

The six Single-Terrains' specific parameters are shown in Table A1. For the Gap, the Size_range represents the platform that robots can stand, the gap robots need to cross is [0.2, 0.3]. For the Parkour, the Height_range will not use the curriculum, it is the range of the parkour height.

Table A1: **Single-Terrain curriculum parameter.** We designed different curriculum parameters for different Single-Terrains.

	Parameter	Height_range(m)	Size_range(m)	Subsection_nums	Tilt_angle(angle)
	Flat	-	-	-	-
	Uneven	[0.10, 0.20]	[0.40, 0.70]	[150, 200]	-
	Stair	[0.15, 0.30]	[0.40, 0.20]	[5, 10]	-
Single Terrain	Gap	-	[0.6, 0.4]	[5, 10]	-
	Bridge	-	[0.40, 0.20]	-	-
	Parkour	[-0.20, 0.20]	[1.00, 0.80]	[3, 8]	[10, 30]

For the **Multi-Terrain**, they are composed of Single-Terrains, the parameters of a single terrain are shown in the Table A1. In addition, Multi-Terrains have platform sizes at the junction, representing the flat part between the two terrains for transition. The platform size has a curriculum design, the parameter is [1.0, 0.0].

Due to the particularity of the four Unseen-Terrains, I will introduce each terrain separately.

- The Gap-Bridge is a superposition of gap and bridge. Based on the gap, the width of the standing platform is set to be the same as our bridge to test the degree of integration of the two strategies of the robot, the detailed curriculum parameters are the superposition of the two single terrains.
- Slope-Bridge is a bridge whose height is set according to the first half of the sine function. The slope of an arch bridge is determined by the length and amplitude of the terrain. Since we have fixed the length of the terrain to 18 meters, the amplitude is set to [1.5, 2.5] meters, with the width as a single bridge. This terrain is designed to test the robot's ability to generalize from stair terrain to slopes.
- Wave-Gap adds several sinusoidal functions to the Gap to make the ground undulate. The parameters of the gap part are the same as those of a single gap, with the addition of the number of waves, the number of sine functions [5, 10], and the amplitude of each sine function [1.5, 2.0]. This terrain is designed to test whether the robot can correctly perform corresponding actions and maintain stability under irregular gaps.
- The Wave-Bridge adds several sinusoidal functions to the bridge to make the ground undulate. The parameters of the bridge part are the same as those of a single bridge, with the addition of the number of waves, the number of sine functions [5, 10], and the amplitude of each sine function [1.5, 2.0]. This terrain is designed to test whether the robot can maintain a stable center of gravity when facing disturbances from irregular ground when walking on a single bridge.

Detailed expert data collection. We collected expert data from three episodes in six terrains, five rounds each, and 1024 environments, totaling about 75M frames of data. In each frame, we record the following information, as shown in the Table A2.

B.2 Details of Specialized Policy Learning

Model Architecture For each specialized ideal policy, we formulate it using an MLP as the backbone \mathcal{F} of the actor. Perceptive scandot is encoded by an MLP encoder $\mathcal{E}_{terrain}$. Apart from that, an RNN-based encoder \mathcal{E}_{hist} is applied to construct the latent information of the history state sequence, details of model architecture are listed in Table A3.

Table A2: Robot Expert Information

Actions	(T,12)
Heightmap	(T,396)
Observations	(T,51)
Rewards	(T,4)
Dof_states	(T,12,2)
Rigid_body_states	(T,13,13)

The actor is formulated as:

$$a_t = \mathcal{F}\left(\mathcal{E}_{\text{hist}}(o_t^{\text{hist}}), \mathcal{E}_{\text{scan}}(o_t^{\text{percep}}), o_t^{\text{proprio}}, c_t, a_{t-1}\right). \tag{11}$$

The critic is also formulated as a MLP $\ensuremath{\mathcal{C}}$:

$$v_t = \mathcal{C}\left(\mathcal{E}_{\text{hist}}(o_t^{\text{hist}}), \mathcal{E}_{\text{scan}}(o_t^{\text{percep}}), o_t^{\text{proprio}}, c_t, a_{t-1}\right). \tag{12}$$

The reinforcement learning algorithm used to train the HMI-conditioned policy is Proximal Policy Optimization Algorithm [74]. The hyperparameters of the PPO Algorithm are listed in Table A4 of the supplementary. We use the same hyperparameters for the training of all specialized policies.

Table A3: Specialized Policy Structure

Parameter	Value
Actor Hidden Dims Critic Hidden Dims	. , ,
Scan Encoder Dims RNN Hidden Size	[128, 64, 32] 512
RNN Layers	1

Table A4: PPO Hyperparameters for Specialized Policy Training

Hyperparameter	Value
Clip range	0.2
GAE discount factor	0.95
Entropy coefficient	0.01
Max gradient norm	1.0
Learning rate	2e-4
Reward discount factor	0.99
Initial policy std	1.0
Minimum policy std	0.2
Number of environments	2048
Number of environment steps per training batch	24
Learning epochs per training batch	5
Number of mini-batches per training batch	4

Reward Functions for Specialized Policy A walk policy is first trained from scratch through reinforcement learning. Subsequently, a series of terrain-specific policies is developed for individual challenging terrains. To enable this progressive learning capability, we design two distinct reward categories. Basic locomotion rewards, as illustrated in Table A5, which enforces fundamental kinematic constraints and penalizes excessive joint torque/velocity for feasible actuator commands. Apart from that, we design specialized rewards for challenging terrains, as shown in Table A6, to provide harder constraints on various scenarios.

B.3 Details of Autoregressive Diffusion Planner

Terrain-Aware Autoregressive Diffusion Training To bridge the gap between training and autoregressive inference, we employ a three-stage scheduled training [66, 78, 79] curriculum. In our

Table A5: Basic Reward Functions and Weight (Notations: v=velocity vector, ω =angular velocity, yaw=heading angle, F=contact force, θ =joint angle, τ =torque, h=height, a=action, $\mathbb{I}(\cdot)$ =indicator function)

Reward Function	Formula	Weight
Orientation	$\sum (g_x^2 + g_y^2)$	-1.0
DOF Acceleration	$\sum \left(rac{\dot{ heta}_t - \dot{ heta}_{t-1}}{\Delta t} ight)^2$	-2.5e-7
Collision	$\sum \mathbb{I}(\ \dot{F}_{\text{contact}}\ \stackrel{\prime}{>} 0.1)$	-10.0
Action Rate	$ a_t - a_{t-1} $	-0.1
Delta Torques	$\sum (au_t - au_{t-1})^2$	-1.0e-7
Torques	$\sum au^2$	-0.00001
DOF Error	$\sum (\theta - \theta_{\text{default}})^2$	-0.04
Feet Stumble	$\mathbb{I}(\ \overline{F_{\text{horizontal}}}\ > 4 F_z)$	-1.0
Base Height	$(h_{ m base}-h_{ m target})^2$	-20.0
Smoothness	$ a_t - a_{t-1} + (a_t - a_{t-1}) - (a_{t-1} - a_{t-2}) $	-0.005
Alive Bonus	\sum (survival)	0.005

Table A6: Special Reward Functions and Weight.

Reward Function	Formula	Weight
Tracking Goal Velocity	$\min\left(rac{oldsymbol{v}_{ ext{cur}}\cdotoldsymbol{v}_{ ext{target}}}{\ oldsymbol{v}_{ ext{target}}\ },v_{ ext{cmd}} ight)/v_{ ext{cmd}}$	3.0
Tracking Yaw	$\exp(- \hat{yaw}_{\text{target}} - \hat{yaw} ^2/0.25)$	0.5
Linear Velocity Z	v_z^2	-1.0
Angular Velocity XY	$\sum (\omega_x^2 + \omega_y^2)$	-0.05
Hip Position	$\sum (\overline{\theta}_{hip} - \theta_{ ext{default}})^2$	-0.5
Feet Edge	$\sum \mathbb{I}(\text{foot_on_edge}) \times \mathbb{I}(\text{terrain_level} > 3)$	-1.0
Feet Parallel	$\sum heta_{ m pitch}^2$	-1.0
Huge Step	$\sum abs(x_{\text{left_ankle}} - x_{\text{right_ankle}})$	0.001
Feet Yaw	$\sum (yaw_{\text{ankle}})^2$	-2.
Feet Dis	$\sum \left((y_{left_ankle}) - (y_{right_ankle}) \right)^2$	-0.001
Knee Dis	$\sum ((y_{\text{left_knee}}) - (y_{\text{right_knee}}))^2$	-0.001
Goal	$\sum (goal)$	0.0002
Knee Foot	$\sum ((y_{knee}) - (y_{ankle}))^2$	-0.001
Foot Height	$\sum (z_{ m ankle})$	0.01
Foot Air Time	$\sum (t_{\text{foot_contact==0}})$	10

terrain-aware autoregressive diffusion planner, we organize training data into overlapping motion windows of fixed length H and slide them through each sequence. At each training iteration iter, we compute a rollout probability p in Alg. 1. We set a maximum of 4 consecutive rollouts during each update to stabilize training and prevent error accumulation.

In our terrain-aware autoregressive diffusion planner, we adopt a complementary three-phase annealing: at each iteration, we sample the history from prior model predictions with probability p and from the ground truth with probability 1-p, gradually increasing p from 0 to 1:

- Fully supervised phase. p=0. Always use ground-truth history, which is fully teacher-forced.
- Scheduled Training Phase. p linearly increases from 0 to 1. With probability p, replace the ground-truth history with the model's own rollout history; otherwise keep ground truth.
- Rollout Training Phase. p = 1. Always use rollout history, which is fully autoregressive.

This simple curriculum likewise exposes the model to its inference-time distribution early in training, improving long-horizon stability and preventing sequence drift. The training algorithm is shown in Alg. 2.

Algorithm 1 Compute schedule rollout probability

```
1: Input: current iteration step iter, number of iteractions in the fully supervised phase I_1, number
   of iterations in scheduled phase I_2
   Output: probability p
3: function SCHEDULE_PROBABILITY(iter, I_1, I_2)
      if iter \leq I_1 then
                                                                   4:
          p \leftarrow 0
5:
      else if iter > I_1 + I_2 then
                                                                    6:
7:
                                                                 8:
      p \leftarrow \tfrac{iter-I_1}{I_2} end if
9:
10:
11:
      return p
12: end function
```

Algorithm 2 Scheduled training for terrain-aware auto-regressive diffusion

1: **Input:** denoiser \mathcal{G}_{θ} with parameters θ , humannoid state dataloader \mathcal{X} , terrain dataloader \mathcal{Y} , total diffusion steps N, consecutive window number T, optimizer \mathcal{O} , training loss \mathcal{L} , max iteration I_{max} , num of iteractions in the fully supervised phase I_1 , num of iterations in scheduled phase I_2 , auto-regressive diffusion sampler \mathcal{S} .

```
2: iter \leftarrow 0
 3: while iter < I_{max} do
               [\mathbf{x}_0, \mathbf{x}_1, ..., \mathbf{x}_T] \sim \mathcal{X}, [y_0, y_1, ..., y_T] \sim \mathcal{Y} \triangleright Sample T trajectory windows from dataset
 4:
              for t \leftarrow 1 to T do
 5:
                                                                                                                                                    Number of rollouts
                     \mathbf{x}_t^0 \leftarrow \mathbf{x}_t
 6:
                     n \sim \mathcal{U}[0, N)
 7:
                     \mathbf{x}_t^n \leftarrow \text{FORWARD\_DIFFUSION}(\mathbf{x}_t^0, n)
 8:

\hat{\mathbf{x}}_{t}^{t} = \mathcal{G}_{\theta}(\mathbf{x}_{t}^{n}, \mathbf{x}_{t-1}, t, y_{t}) \\
\nabla \leftarrow \nabla_{\theta} \mathcal{L}(\mathbf{x}_{t}^{0}, \hat{\mathbf{x}}_{t}^{0})

 9:
                                                                                                                                                  Next state denoising
10:
                      \theta \leftarrow \mathcal{O}(\theta, \nabla)
11:
                                                                                                                                                       ▶ Back propagation
                     p \leftarrow \text{SCHEDULE\_PROBABILITY}(iter, I_1, I_2) \quad \triangleright \text{Sample schedule training probability}
12:
                      if rand() < p then
13:
                            \begin{aligned} \mathbf{x}_t^N &\leftarrow \text{Forward\_diffusion}(\mathbf{x}_t^0, N) \\ \tilde{\mathbf{x}}_t^0 &= \mathcal{S}(\mathcal{G}_{\theta}, \mathbf{x}_t^N, \mathbf{x}_{t-1}, N, y_t) \\ \mathbf{x}_t &\leftarrow \tilde{\mathbf{x}}_t^0 \end{aligned} \quad \triangleright \text{ Set pi}
14:
                                                                                                                                                    ⊳ Full trajectory sampling loop
15:
                                                                                                          > Set predicted state trajectory into history
16:
17:
                           \mathbf{x}_t \leftarrow \mathbf{x}_t^0
18:
                                                                                                                                          19:
20:
                     iter \leftarrow iter + 1
21:
              end for
22: end while
```

Implementation Details of Diffusion Models. The denoiser \mathcal{G} is implemented on the DIT backbone with 8 Transformer decoder layers (hidden size 512). We apply classifier-free guidance by masking the terrain embedding with probability 0.1 during both training and inference. Local terrain is encoded from a 396-egocentric height map using lightweight MLP blocks. The final feature map is flattened and projected to a 256-dimensional terrain embedding.

We train for a total of 300K diffusion iterations on our expert locomotion dataset, selecting the best checkpoints at 250K for validation. Optimization is via Adam with batch size 1024. All models run on a single NVIDIA GeForce RTX 4090 GPU for nearly 30 hours, and at test time, we use DDPM sampling with guidance scale $\omega = 5$ to autoregressively generate continuous trajectories in real time.

B.4 Details of HMI-conditioned Unified Policy

Model Architecture. The network architecture is inherited from B.2. Different from a specialized policy network, HMI-condition policy network contains a RNN future encoder $\mathcal{E}_{\text{future}}$, which encodes

predict state sequence $g_t \in \mathbb{R}^{d \times H}$ sampled from the diffusion planner. The architecture of the HMI-conditioned unified policy is formulated as:

$$a_t = \mathcal{F}\left(\mathcal{E}_{\text{hist}}(o_t^{\text{hist}}), o_t^{\text{proprio}}, \mathcal{E}_{\text{future}}(g_t), c_t, a_{t-1}\right). \tag{13}$$

Reward Functions for Unified Policy. Different from reward functions during specialized policy training, in this phase, we use unified rewards for training a tracking policy. The short-term reward functions are listed in Table A7. We conduct short-term tracking reward functions using formulas described in [22], in which the task reward aims to achieve successful whole-body tracking in real-time. In this work, we only need to control the lower body. To fully leverage predicted motion sequences rather than using single-frame tracking losses as in conventional approaches, our method introduces an AMP-style [75] adversarial reward with a key differentiation: instead of relying on pre-recorded motion clips or datasets, we update the discriminator using future state sequences online-sampled from the diffusion planner, as described in Algorithm 3, this long-term reward is described in equation 7. This AMP-style reward enables:

- Temporal-Consistent Tracking: the policy learns to match the diffusion-generated motion patterns over extended horizons;
- Dynamic Style Adaptation: the discriminator compares rollout segments against diffusionplanned state sequences rather than static reference motions.

Table A7: Short-term Reward Functions and Weight for HMI-conditioned Unified Policy.

Reward Function	Formula	Weight
Joint position	$\exp(-0.25\ \theta_t - \hat{\theta}_t\ _2)$	3.0
Joint velocity Keypoint position	$\exp(-0.25\ \hat{\theta}_t - \hat{\theta}_t\ _2^2) \\ \exp(-0.5\ \hat{p}_t - p_t\ _2^2)$	3.0 5.0
Keypoint rotation Base linear velocity	$\exp(-0.1\ \hat{p}_t - p_t\ _2) \\ \exp(-10.0\ \hat{p}_t - \hat{p}_t\ _2)$	1.5 8.0
Base angular velocity	$\exp(-0.01\ \hat{v}_t - v_t\ _2)$	8.0

DreamPolicy Inference Process. The inference process is addressed in Algorithm 4: the agent first observes the current state s_t from the environment and acquires the terrain heightmap, stores the current state in the history buffer, then interacts with the environment to obtain the action, executes the action, and finally transitions to the next state s_{t+1} .

C Additional Experiments and Results

C.1 Detailed Implementation of Baselines

Vanilla Actor-Critic. As introduced in [83], we use the naive implementation of legged_gym and rsl_rl. In which we use only regularization rewards and velocity-tracking rewards for PPO training without specialized reward design.

Scenario Specialized Policy. Inspired by [3], we use a scandot encoder and a privileged information estimator, as mentioned in Section B.2. To this end, we will not use this setting for experiments on multi-terrains.

Distillation-based Method. Inspired by [4], which trained a unified policy using online distillation via DAgger [84]. We trained a policy via online distillation, where the unified policy learn from multiple single specialized policies via supervision.

Ablation on Diffusion Planner. In this setting, we remove the autoregressive diffusion planner, which provides humanoid motion imagery to the HMI-conditioned unified policy. Due to the lack of humanoid motion imagery, we train the discriminator using the standard implementation of AMP [75], in which we sample transitions from offline trajectories collected from specialized policies.

Algorithm 3 Training with Online Diffusion AMP

```
1: Input \mathcal{M}_{planner}: autoregressive diffusion planner, K: history length, H: horizon
 2: D \leftarrow initialize discriminator
 3: \pi \leftarrow initialize policy
 4: V \leftarrow initialize value function
 5: \mathcal{B} \leftarrow \emptyset initialize replay buffer
 6: \mathcal{H} \leftarrow \emptyset initialize history buffer
 7: while not done do
              for trajectory i = 1, ..., m do
                                                                                                                                          Data collection phase
 8:
                    \tau^i \leftarrow \emptyset
 9:
                    for step t = 0, ..., T - 1 do
10:
                           Execute a_t \sim \pi(s_t), observe s_{t+1}, store (s_t, a_t, r_t^{\text{base}}, s_{t+1}) in \mathcal{B} Update \mathcal{H} with s_t \colon \mathcal{H} \leftarrow \text{concat}(\mathcal{H}[-K+1:], s_t) \triangleright Main
11:
                                                                                                                                   \triangleright Maintain latest K states
12:
13:
                            if t < K - 1 then
                                                                                                                                    ▶ Padding for initial phase
                                   \hat{\mathcal{H}} \leftarrow [s_0, ..., s_0, \mathcal{H}[0:t+1]]
14:
                                                                                                                                                            \triangleright Pad with s_0
15:
                            else
                                  \hat{\mathcal{H}} \leftarrow \mathcal{H}[-K:]
16:
                                                                                                                                                         \triangleright Last K states
                            end if
17:
                            Generate \{\hat{s}_{t+1:t+H}\} \sim \mathcal{M}_{planner}(\hat{\mathcal{H}})
18:
                           \begin{array}{l} d_t \leftarrow D(\Phi(s_t), \Phi(\hat{s}_{t+1})) \\ r_t^{\text{amp}} \leftarrow \text{style reward via Eq.7 using } d_t \\ r_t \leftarrow w^{\text{base}} r_t^{\text{base}} + w^{\text{goal}} r_t^{\text{goal}} + w^{\text{amp}} r_t^{\text{amp}} \\ \text{Append } (s_t, a_t, r_t, s_{t+1}) \text{ to } \tau^i \end{array}
19:
                                                                                                                                  20:
21:
22:
23:
                    end for
              end for
24:
25:
              for update step = 1, ..., n do
                                                                                                                                                      ▶ Training phase
                    b^{\pi} \leftarrow \text{sample } K \text{ transitions } \{(s_j, s'_j)\}_{j=1}^K \text{ from } \mathcal{B}
26:
                    Generate \{\hat{s}_{j:j+H}\}_{j=1}^K \sim \mathcal{M}_{\text{planner}}(b^{\pi})
Update D via Eq.9 using \{(\Phi(s_j), \Phi(\hat{s}_{j+1}))\}_{j=1}^K
27:
                                                                                                                                         ▷ On-the-fly generation
28:
                                                                                                                                                       ▶ Fresh samples
                     Update V and \pi using \{\tau^i\}_{i=1}^m
29:
                                                                                                                                             ▶ Policy optimization
30:
              end for
31: end while
```

Ablation on HMI-conditioned RL. In this setting, we use the action output by the autoregressive diffusion planner directly rather than state predictions for RL guidance. This setting aims to demonstrate that diffusion directly predicts actions with poor performance, as illustrated in C.2, therefore, using prediction and reinforcement learning training on more continuous state spaces can achieve dynamically feasible multi-terrain adaptation.

C.2 Additional Experiments

Table C.2 shows the detailed data on a single terrain that we display using radar maps in the main text. The detailed data shows that our method does not exhibit significant performance degradation. Although the success rate of the distillation method is higher than ours on the gap terrain, our complete rate is higher, which means that there may be a problem in the initialization part of the model, resulting in a decrease in the success rate.

We test all methods in the additional multi-terrain environments. Across all combinations of the two terrain types, it consistently outperforms other approaches, shown in Table A9 A10 A11. This shows that our algorithm has strong generative planning capabilities when switching between different terrains.,k

C.3 Additional Visualization Results

Additional visualization results of multi-terrain has shown in Figure A1, A2, A3, A4 sequentially. Visualization results of unseen-terrain has shown in Figure A5, A6, A7, A8.

Algorithm 4 DreamPolicy Inference

```
1: Input \mathcal{M}_{planner}: trained diffusion planner, \pi: trained policy, K: history length, H: horizon
 2: \mathcal{H} \leftarrow \emptyset initialize history buffer
 3: z_{\text{terrain}} \leftarrow \text{preprocessed terrain heightmap}
     while running do
          Observe current state s_t
 5:
          Update \mathcal{H}: \mathcal{H} \leftarrow \text{concat}(\mathcal{H}[-K+1:], s_t)
                                                                                                 \triangleright Maintain latest K states
 6:
 7:
          if |\mathcal{H}| < K then
                                                                                                     ▶ Initial phase padding
               \hat{\mathcal{H}} \leftarrow [s_0, ..., s_0, \mathcal{H}[0:t+1]]
 8:
                                                                                                      ⊳ Pad with initial state
 9:
              \hat{\mathcal{H}} \leftarrow \mathcal{H}[-K:]
                                                                                                               \triangleright Last K states
10:
11:
          Generate \{\hat{s}_{t+1:t+H}\} \sim \mathcal{M}_{planner}(\mathcal{H}, z_{terrain})
                                                                                        12:
          Construct policy input: \tilde{s}_t \leftarrow [s_t; \hat{s}_{t+1:t+H}]
                                                                                        13:
14:
          a_t \leftarrow \pi(\tilde{s}_t)
                                                                                                            ▶ Generate action
15:
          Execute a_t on robot and observe next state s_{t+1}
16: end while
```

Table A8: **Settings Comparison in Single-Terrain**. All data in the table are shown as percentages; the higher the better. The best results are highlighted in boldface.

	Uneven		Bridge		St	Stair		Parkour		Flat		Gap	
	R_{succ} (%)	R _{cmp} (%)	$R_{\rm succ}$ (%)	R _{cmp} (%)	R_{succ} (%)	R _{cmp} (%)	R_{succ} (%)	$R_{\rm cmp}$ (%)	R_{succ} (%)	$R_{\rm cmp}$ (%)	R_{succ} (%)	R _{cmp} (%)	
Vanilla Specialized Policy										$95.33{\scriptstyle\pm2.15}\atop99.99{\scriptstyle\pm0.00}$			
Distillation Ours										$\begin{array}{c} \textbf{100.00} {\pm} 0.00 \\ \textbf{100.00} {\pm} 0.00 \end{array}$			
Ours w/o Diffusion Ours w/o GCRL										99.27±0.06 100.00 ±0.00			

Table A9: **Performance Comparison in Multi-terrain.** All data in the table are shown as percentages, the higher the better. The best results are highlighted in boldface.

	Parkour&Uneven		Parkour	&Bridge	Parkou	r&Stair	Parkour&Gap	
	$R_{\rm succ}(\%)$	$R_{\rm cmp}(\%)$	$R_{\rm succ}(\%)$	$R_{\rm cmp}(\%)$	$R_{\rm succ}(\%)$	$R_{\rm cmp}(\%)$	$R_{\rm succ}(\%)$	$R_{\rm cmp}(\%)$
Vanilla	0.00 ± 0.00	4.98 ± 0.48	0.00 ± 0.00	$6.25 {\pm} 0.15$	0.00 ± 0.00	$5.22{\pm}0.56$	0.00 ± 0.00	$5.14{\pm}0.36$
Distillation	$12.37{\pm0.86}$	$46.16{\pm}1.72$	$13.42{\pm}0.36$	$51.33{\pm}0.28$	$51.33{\pm}0.19$	$88.34{\pm}0.21$	$61.15{\pm}0.11$	$92.16{\pm}0.46$
Ours	65.44 ± 0.14	76.35 ± 0.24	35.32 ± 0.07	63.25 ±0.16	70.38 ± 0.02	92.33 ± 0.08	80.36 ± 0.08	97.25 ±0.16

Table A10: **Performance Comparison in Multi-terrain.** All data in the table are shown as percentages, the higher the better. The best results are highlighted in boldface.

	Stair&Uneven		Stair&Bridge		Stair&Gap	
	$R_{ m succ}(\%)$	$R_{\rm cmp}(\%)$	$R_{ m succ}(\%)$	$R_{\rm cmp}(\%)$	$R_{ m succ}(\%)$	$R_{\rm cmp}(\%)$
Vanilla	7.18±0.45	31.45±1.79	8.33±0.28	44.36 ±0.45	7.62 ± 0.21	39.74 ±0.33
Distillation	62.36 ± 0.45	87.28 ± 1.62	21.64 ± 0.62	52.17 ± 1.06	74.52 ± 0.56	89.05 ± 0.30
Ours	73.16 ±0.24	94.25 ±0.15	41.18 ±0.06	75.15 \pm 0.14	76.74 ±0.06	91.38 ±0.45

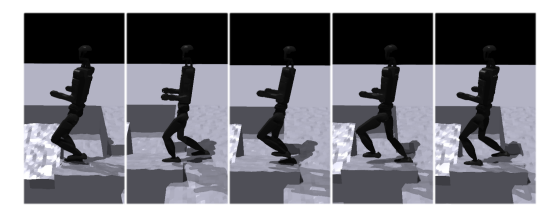
D Supplementary Video

We have included a video in the supplementary material to summarize our main contributions and present video results of humanoid locomotion. More details are as follows.

• We introduced our DreamPolicy algorithm framework, summarized our main contributions from four aspects and introduced each part of the DreamPolicy framework in detail.

Table A11: Performance Comparison in Multi-terrain. All data in the table are shown as percentages, the higher the better. The best results are highlighted in boldface.

	Bridge&Uneven		Bridge&Gap		Uneven&Gap	
	$R_{ m succ}(\%)$	$R_{\rm cmp}(\%)$	$R_{ m succ}(\%)$	$R_{\rm cmp}(\%)$	$R_{ m succ}(\%)$	$R_{\rm cmp}(\%)$
Vanilla	$11.17{\pm}1.28$	$62.19{\pm}2.34$	0.00 ± 0.00	$48.34{\pm}0.15$	$13.16{\pm}1.58$	$71.34{\pm}4.52$
Distillation	$71.35{\pm}0.28$	$76.33{\pm}1.58$	$15.34{\pm}0.25$	$62.36{\pm}1.28$	$71.42{\pm}0.54$	$79.32{\pm}1.26$
Ours	84.16 ± 0.17	92.55 ± 0.32	44.15 ±0.01	72.58 \pm 0.04	74.09 ± 0.04	83.18 ± 0.14



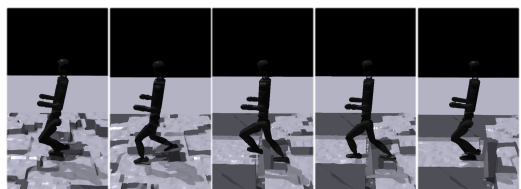


Figure A1: Multi Terrain - Parkour

Figure A2: Multi Terrain - Uneven

- We gave our quantitative results on Single terrain, Multi-terrains, and Unseen-terrains, and analyzed the impact of scale on our method.
- We gave a visual comparison of our performance on different terrains with the traditional distillation method, showing that our algorithm has significant advantages.

Extended Limitation and Discussions

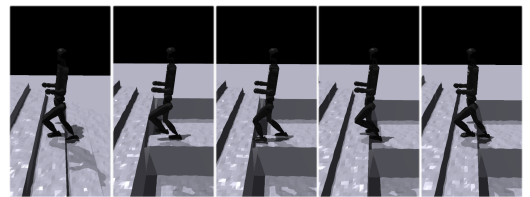
E.1 Limitation and Failure Cases

We present several illustrative failure cases (see Fig. A9 and Fig. A10), in which the robot resets due to falling or tumbling on challenging terrains, yet ultimately succeeds in subsequent attempts. Our analysis suggests that the limitations may stem from two factors: 1) Naive terrain encoding. The current diffusion planner employs a plain MLP to process the 396-dimensional structured terrain elevation map, without any spatially aware components that could extract local geometric patterns and contextual cues essential for handling sharp gradients or complex surface discontinuities. 2) Limited policy perception. Our HMI-conditioned unified policy relies exclusively on the planner's state trajectory predictions for navigation, lacking any direct perception of the terrain. Consequently, the policy is unable to react to unforeseen geometric perturbations or dynamically adjust its foot placement in extreme, unstructured environments.

These combined limitations—inadequate feature representation of challenging terrain and absence of real-time sensory feedback—undermine stability and recovery capability.

E.2 Discussion and Future Work

We propose a set of comprehensive research directions and rigorous validation studies—spanning dataset augmentation, terrain-generalization techniques, inference optimization, and real-world



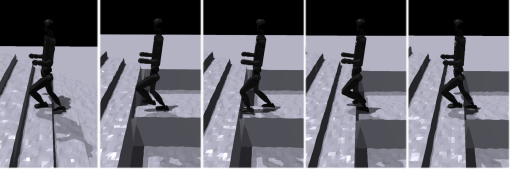




Figure A3: Multi Terrain - Bridge

Figure A4: Multi Terrain - Gap

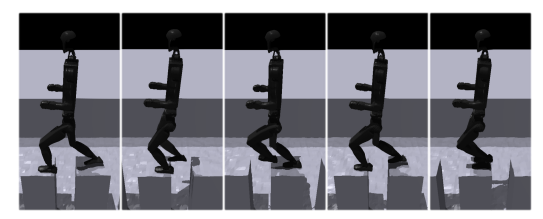
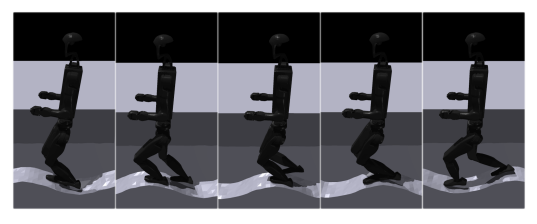


Figure A5: Gap-Bridge Terrain

Figure A6: Slope-Bridge Terrain



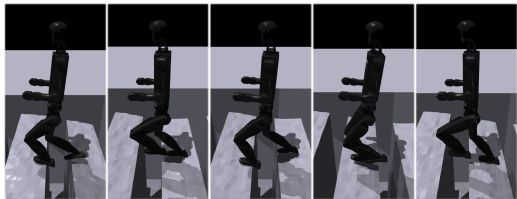


Figure A7: Wave Bridge Terrain

Figure A8: Wave Gap Terrain

robotic trials—to systematically extend the capabilities and verify the practical effectiveness of our diffusion-based humanoid motion planning framework:

- Augment dataset diversity. Integrate additional data sources beyond the current set of expert policies trained in RL—including demonstrations from varied control algorithms, motion capture recordings of human subjects, and synthetic trajectories generated under different environmental perturbations—to significantly enrich the breadth, variability, and robustness of the humanoid motion imagery dataset.
- Enhance terrain generalization. Develop and evaluate advanced terrain-encoding strategies—such as learned geometric embeddings, height-map spectral features, and multimodal descriptors—that can effectively generalize across a wide spectrum of previously unseen environments, thereby enabling the diffusion planner to produce reliable, accurate future-state priors even on novel or complex terrains.
- Accelerate inference efficiency. Reduce sampling latency by integrating techniques such as
 step-reduction schedulers, diffusion model distillation into lightweight student networks,
 dynamic stopping criteria based on convergence metrics, or adaptive iteration strategies
 that allocate computation where it is most needed, all aimed at supporting true real-time
 deployment on computationally constrained hardware.
- **Deploy DreamPolicy on real-world robotics.** Validate and refine the diffusion planner on physical humanoid platforms—by conducting extensive trials under varying payloads, actuator latencies, and surface conditions—to rigorously assess transfer efficacy, safety guarantees, and control stability when operating under real-world operational constraints and hardware imperfections.
- Standardize benchmarking. Develop comprehensive, open evaluation suites—comprising
 diverse task scenarios, standardized test terrains, and reproducible performance metrics (e.g.
 success rate, energy consumption, and robustness measures)—to facilitate fair, transparent
 comparisons across diffusion-based humanoid planners and to drive accelerated community
 progress.

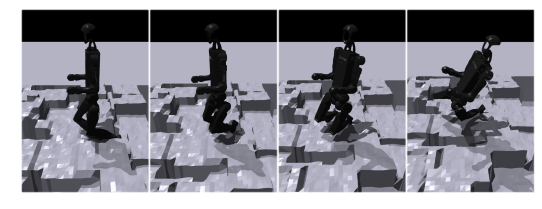




Figure A9: Failure Case on multi-Terrain.

Figure A10: Failure Case on Unseen Terrain.